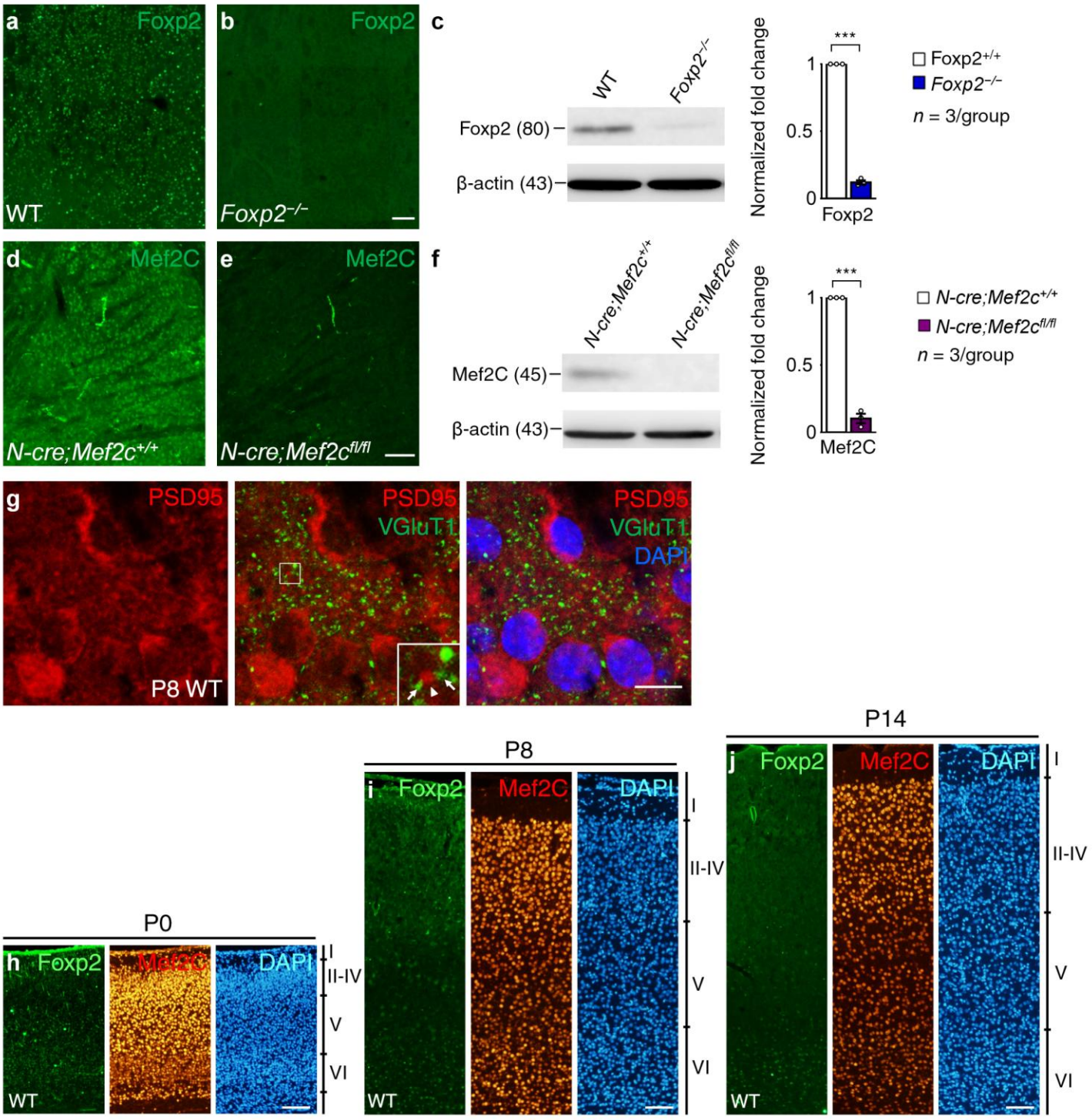

Supplementary Figure 1

Specificity of Foxp2 and Mef2C antibodies and postnatal development of Foxp2 and Mef2C in neocortex.

(**a-f**) Foxp2 and Mef2C immunoreactive signals are barely detectable in *Foxp2*$^{-/-}$ knockout striatum (**a-c;** Student's *t* test, $t_{(4)} = 56.963$, $P = 0.000001$) and *Nestin-cre;Mef2c*$^{fl/fl}$ knockout striatum (**d-f;** $t_{(4)} = 24.504$, $P = 0.000016$), as assayed by immunofluorescence staining and Western blotting. Scale bars, 100 μm. Error bars represent s.e.m. ***$P < 0.001$. Images and data represent three mice per genotype. (**g**) Corticostriatal terminals marked by VGluT1 (green) form putative synapses with PSD95 (red) in P8 striatum. Inset in the

middle panel shows adjacent presynaptic VGluT1-positive (green, arrows) and postsynaptic PSD95-positive (red, arrowhead) puncta at high magnification. Scale bars, 10 μm. Images represent two repeats. (**h-j**) Foxp2 is predominantly expressed by layer VI neurons, whereas Mef2C is expressed throughout the primary motor cortex at P0 (**h**), P8 (**i**) and P14 (**j**). Scale bars, 100 μm. Images represent two repeats.

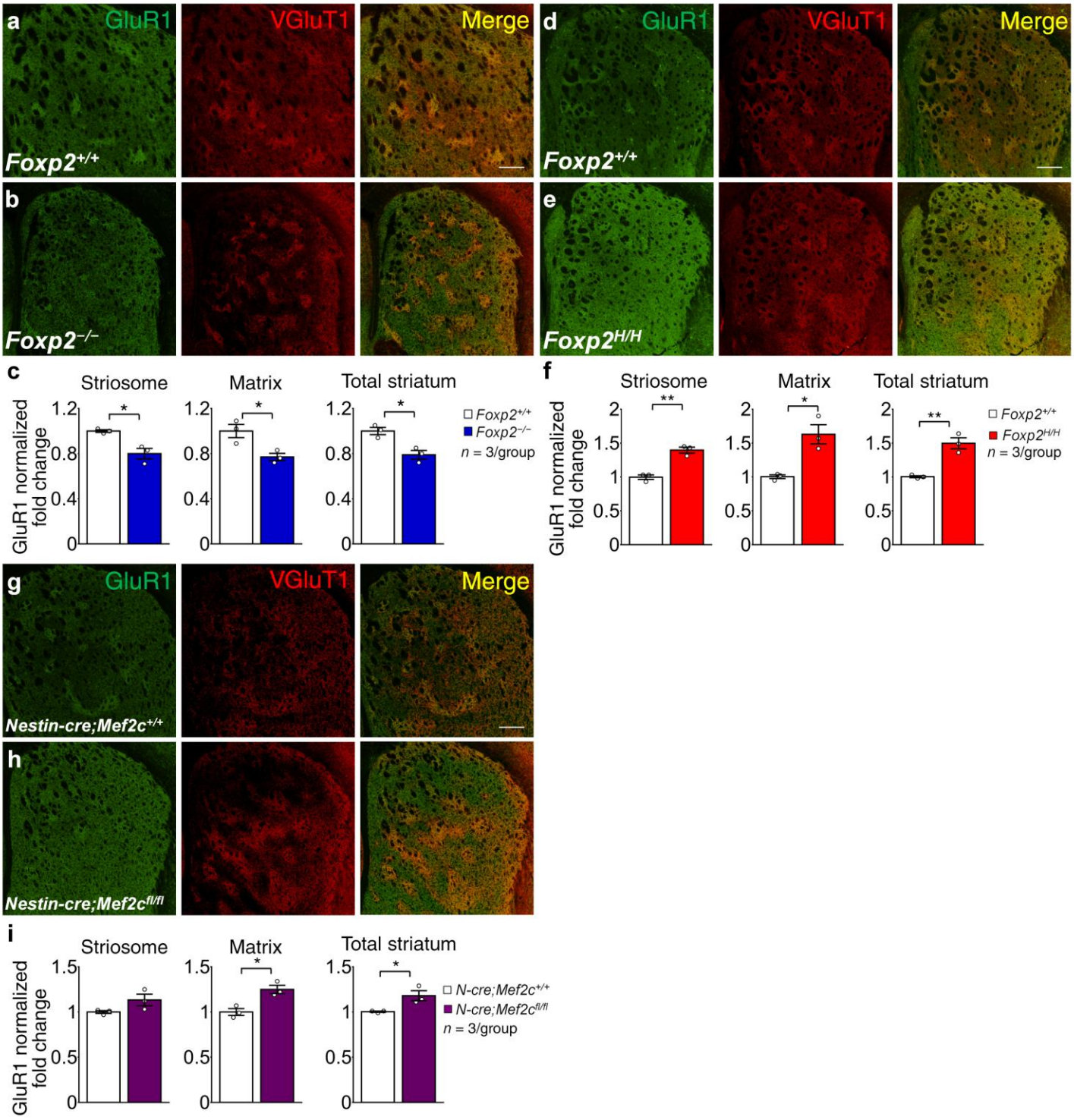

Supplementary Figure 2

GluR1 immunostaining in the striatum of *Foxp2*$^{-/-}$, *Foxp2*$^{H/H}$ and *Nestin-cre;Mef2c*$^{fl/fl}$ mice.

(**a-c**) Double immunostaining of GluR1 and VGluT1 shows that VGluT1-positive striosomes contain high levels of GluR1 expression in the striatum. GluR1 immunofluorescence intensity is decreased in striosomes ($t_{(4)}$ = 4.228, P = 0.013) and matrix ($t_{(4)}$ = 3.535, P = 0.024), as well as entire striatum ($t_{(4)}$ = 4.298, P = 0.013), of P7 *Foxp2*$^{-/-}$ mice (**b**), compared to wildtype mice (**a**). (**d-f**) By contrast,

GluR1 immunofluorescence intensity is increased in striosomes ($t_{(4)} = -7.426$, $P = 0.002$) and matrix ($t_{(4)} = -4.343$, $P = 0.012$), and in entire striatum ($t_{(4)} = -6.013$, $P = 0.004$), of P8 *Foxp2*$^{H/H}$ mice (**e**), relative to wildtype mice (**d**). (**g-i**) GluR1 immunofluorescence intensity is increased in the matrix ($t_{(4)} = -4.201$, $P = 0.014$) and in the entire striatum ($t_{(4)} = -3.240$, $P = 0.032$) of P8 *Nestin-cre;Mef2c*$^{fl/fl}$ mice (**h**), relative to control *Nestin-cre;Mef2c*$^{+/+}$ mice (**g**). **P* < 0.05, ***P* < 0.01. Error bars represent s.e.m. Scale bars, 200 μm. Images and data represent three mice per genotype.

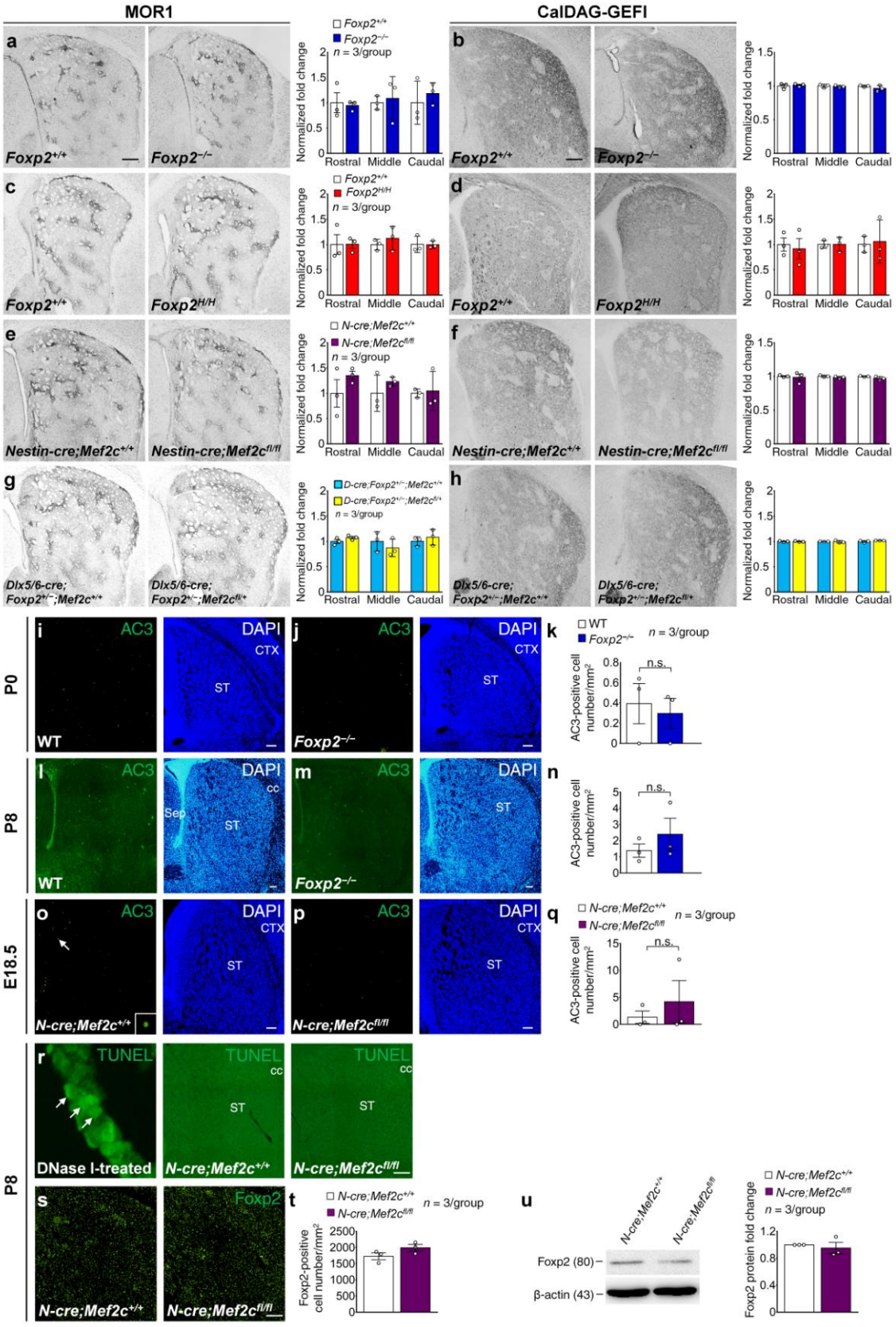

Nature Neuroscience: doi:10.1038/nn.4380

Supplementary Figure 3

Normal striatal compartmentation and a lack of cell death in *Foxp2* and *Mef2c* mutant mice.

(**a-h**) MOR1 and CalDAG-GEFI immunostaining show that the macroscopic patterns and the regions of MOR1-positive striosomes (**a,c,e,g**) and CalDAG-GEFI-enriched matrix (**b,d,f,h**) are not altered in the striatum of P7 *Foxp2*$^{-/-}$ mice (**a,b**), P8 *Foxp2*$^{H/H}$ mice (**c,d**), P8 *Nestin-cre;Mef2c*$^{fl/fl}$ mice (**e,f**) or P8 *Dlx5/6-cre;Foxp2*$^{+/-}$*;Mef2c*$^{fl/+}$ mice (**g,h**), relative to control mice (Student's *t* test, **a**, for rostral, $t_{(4)}$ = 0.257, P = 0.810; for middle, $t_{(4)}$ = -0.334, P = 0.755; for caudal, $t_{(4)}$ = −0.654, P = 0.549; **b**, for rostral, $t_{(4)}$ = −0.505, P = 0.640; for middle, $t_{(4)}$ = 0.330, P = 0.758; for caudal, $t_{(4)}$ = 1.392, P = 0.236; **c**, for rostral, $t_{(4)}$ = −0.035, P = 0.974; for middle, $t_{(4)}$ = −0.816, P = 0.460; for caudal, $t_{(4)}$ = −0.037, P = 0.972; **d**, for rostral, $t_{(4)}$ = 0.350, P = 0.744; for middle, $t_{(4)}$ = −0.037, P = 0.972; for caudal, $t_{(4)}$ = −0.236, P = 0.825; **e**, for rostral, $t_{(4)}$ = −0.035, P = 0.283; for middle, $t_{(4)}$ = −0.816, P = 0.341; for caudal, $t_{(4)}$ = −0.037, P = 0.850; **f**, for rostral, $t_{(4)}$ = 0.210, P = 0.844; for middle, $t_{(4)}$ = 1.029, P = 0.362; for caudal, $t_{(4)}$ = 1.655, P = 0.173; **g**, for rostral, $t_{(4)}$ = −1.501, P = 0.208; for middle, $t_{(4)}$ = 0.873, P = 0.432; for caudal, $t_{(4)}$ = −0.786, P = 0.476; **h**, for rostral, $t_{(4)}$ = 0.157, P = 0.883; for middle, $t_{(4)}$ = 0.374, P = 0.728; for caudal, $t_{(4)}$ = −1.669, P = 0.171). Error bars represent s.e.m. Scale bars, 200 μm. (**i-q**) The number of cells positive for activated caspase 3 (AC3) are not altered in the striatum of P0 (**i-k**, $t_{(4)}$ = 0.390, P = 0.716) and P8 (**l-n**, $t_{(4)}$ = −0.940, P = 0.400) *Foxp2*$^{-/-}$ knockout mice or in the striatum of E18.5 *Nestin-cre;Mef2c*$^{fl/fl}$ knockout mice (**o-q**, $t_{(4)}$ = −0.707, P = 0.519). CTX: cortex; ST: striatum; Sep: septum; cc: corpus callosum. (**r**) TUNEL signals (left) are not detected in the striatum of P8 *Nestin-cre;Mef2c*$^{+/+}$ (middle) or in the striatum of P8 *Nestin-cre;Mef2c*$^{fl/fl}$ (right) mice. Arrows indicate DNase I-treated cells as positive control. (**s,t**) The density of Foxp2-positive cells in *Nestin-cre;Mef2c*$^{fl/fl}$ knockout striatum is similar to that in *Nestin-cre;Mef2c*$^{+/+}$ control striatum ($t_{(4)}$ = −1.800, P = 0.146). (**u**) Consistently, the protein level of Foxp2 is not altered in P8 *Nestin-cre;Mef2c*$^{fl/fl}$ knockout striatum, compared to *Nestin-cre;Mef2c*$^{+/+}$ control striatum ($t_{(4)}$ = 0.569, P = 0.627). Scale bars, 200 μm. Images and data represent three mice per genotype.

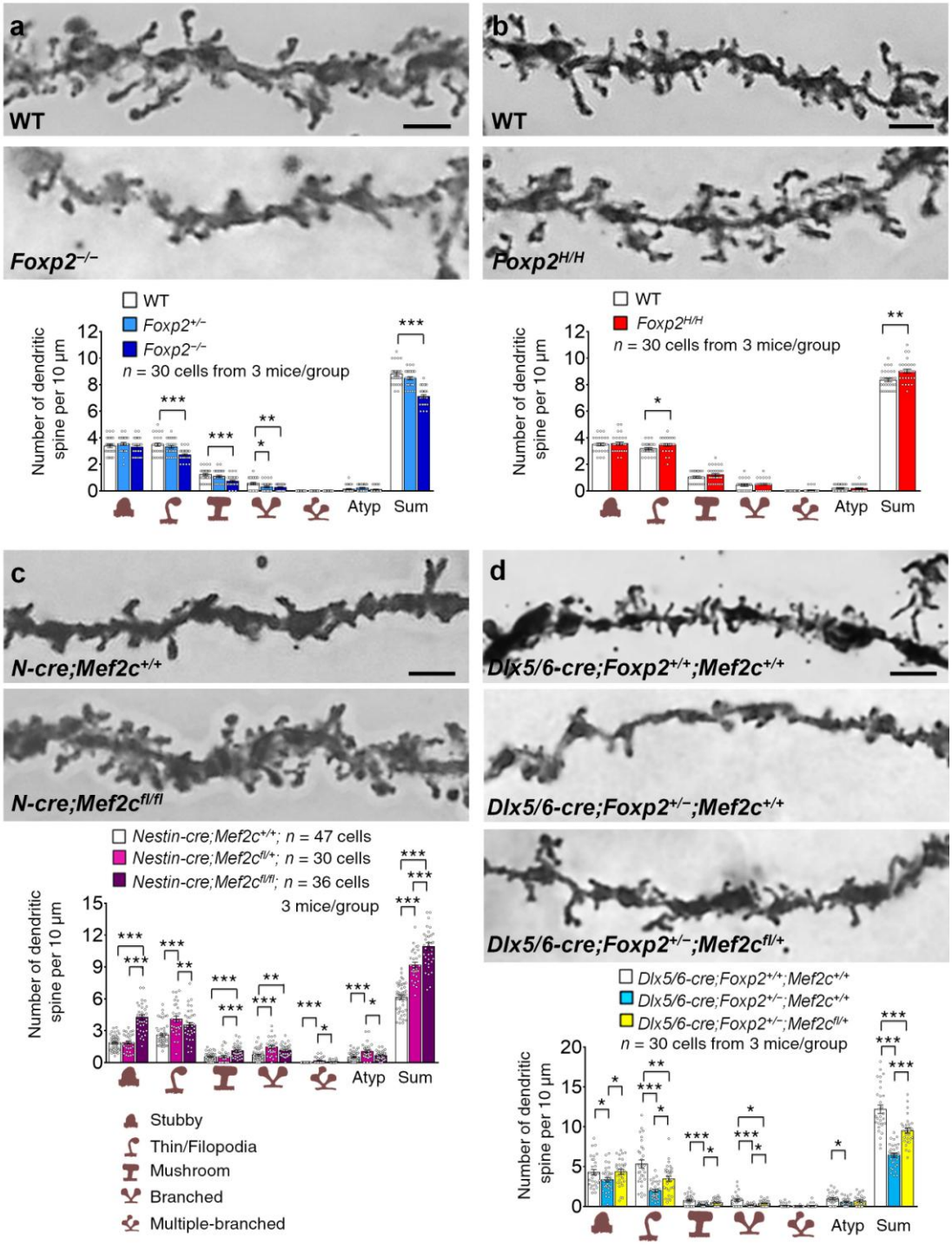

Supplementary Figure 4

Alterations of dendritic spines of SPNs in the dorsomedial striatum of *Foxp2* and *Mef2c* mutant mice.

Dendritic spines of SPNs observed in Golgi-stained sections through the dorsomedial striatum are decreased in the *Foxp2*$^{-/-}$ mice (**a**, for stubby, $F_{(2, 87)} = 1.309$, $P = 0.275$; for thin/filopodia, $F_{(2, 87)} = 15.251$, $P = 0.000002$; for mushroom, $F_{(2, 87)} = 10.333$, $P = 0.000094$; for branched, $F_{(2, 87)} = 6.699$, $P = 0.002$; for atypical, $F_{(2, 87)} = 1.882$, $P = 0.158$; for sum, $F_{(2, 87)} = 28.470$, $P = 0.000000$), but are increased in *Foxp2*$^{H/H}$ mice (**b**, for stubby, $t_{(29)} = -0.421$, $P = 0.677$; for thin/filopodia, $t_{(29)} = -2.134$, $P = 0.041$; for mushroom, $t_{(29)} = -1.670$, $P = 0.106$; for branched, $t_{(29)} = -0.867$, $P = 0.393$; for multiple branched, $t_{(29)} = -1.795$, $P = 0.083$; for atypical, $t_{(29)} = 0.226$, $P = 0.823$; for sum, $t_{(29)} = -4.016$, $P = 0.000383$), in *Nestin-cre;Mef2c*$^{fl/+}$ and *Nestin-cre;Mef2c*$^{fl/fl}$ mice (**c**, for stubby, $F_{(2, 110)} = 61.760$, $P = 0.000000$; for

thin/filopodia, $F_{(2, 110)}$ = 12.941, P = 0.000009; for mushroom, $F_{(2, 110)}$ = 16.513, P = 0.000001; for branched, $F_{(2, 110)}$ = 14.529, P = 0.000003; for multiple branched, $F_{(2, 110)}$ = 9.961, P = 0.000106; for atypical, $F_{(2, 110)}$ = 9.982, P = 0.000105; for sum, $F_{(2, 110)}$ = 86.254, P = 0.000000) and in *Dlx5/6-cre;Foxp2*$^{+/-}$*;Mef2c*$^{fl/+}$ mice (**d**, for stubby, $F_{(2, 89)}$ = 3.391, P = 0.038; for thin/filopodia, $F_{(2, 89)}$ = 22.339, P = 0.000000; for mushroom, $F_{(2, 89)}$ = 8.687, P = 0.000366; for branched, $F_{(2, 89)}$ = 10.016, P = 0.000128; for multiple branched, $F_{(2, 89)}$ = 2.433, P = 0.094; for atypical, $F_{(2, 89)}$ = 3.759, P = 0.027; for sum, $F_{(2, 89)}$ = 57.917, P = 0.000000. Atyp: atypical. One-way ANOVA is used in **a**, **c**, and **d**. Student's *t* test is used in **b**. *P < 0.05, **P < 0.01; ***P < 0.001. Error bars represent s.e.m. Scale bars, 2.5 μm. Data represent at least 30 cells from three mice per genotype.

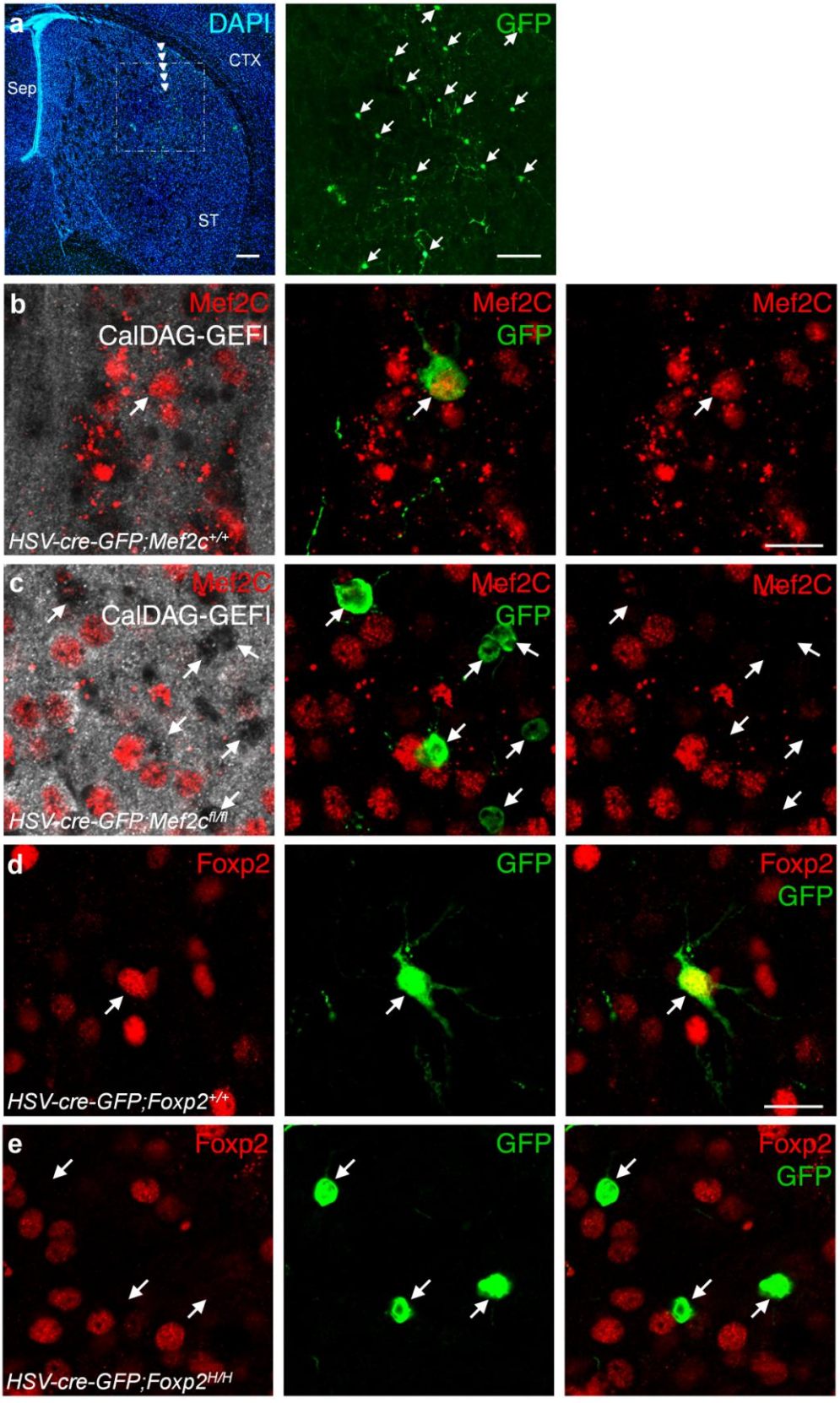
a
DAPI
CTX
Sep
ST
GFP
b
Mef2C
CalDAG-GEFI
HSV-cre-GFP;Mef2c+/+
Mef2C
GFP
Mef2C
c
Mef2C
CalDAG-GEFI
HSV-cre-GFP;Mef2cfl/fl
Mef2C
GFP
Mef2C
d
Foxp2
HSV-cre-GFP;Foxp2+/+
GFP
Foxp2
GFP
e
Foxp2
HSV-cre-GFP;Foxp2H/H
GFP
Foxp2
GFP

Supplementary Figure 5

Validation of HSV-Cre-GFP virus-mediated deletion of humanized *Foxp2* in striatal neurons *of Foxp2*$^{H/H}$ mice and deletion of *Mef2c* in striatal neurons of *Mef2c*$^{fl/fl}$ mice.
(**a**) Intrastriatal injections of HSV-Cre-GFP viruses were made in P2 *Mef2c*$^{fl/fl}$ mice. The boxed region in the left panel, covering the needle track, is shown at high magnification in the right panel. Many GFP-positive cells (arrows in the right panel) are distributed in the region around the needle track (arrowheads in the left panel) in the P8 striatum (ST). CTX, cortex; Sep, Septum. (**b,c**) GFP-positive cells co-expressing Mef2C (arrows) are found in control wildtype mice (**b**), but not in P8 HSV-Cre-GFP;*Mef2c*$^{fl/fl}$ mice (arrows, **c**). The sections are double-immunostained for Mef2C and the striatal matrix marker CalDAG-GEFI (left panels) to identify GFP-positive cells in Mef2C-enriched matrix regions. Images represent six repeats. (**d,e**) Double-immunostaining show co-localization of Foxp2 (red) and GFP in the striatum of P8 HSV-Cre-GFP;*Foxp2*$^{+/+}$ wildtype mice (arrows in **d**), but not in the striatum of HSV-Cre-GFP;*Foxp2*$^{H/H}$ mice (arrows in **e**). Images represent four repeats. Scale bars are 200 μm in **a**, 20 μm in **b** and **d**.

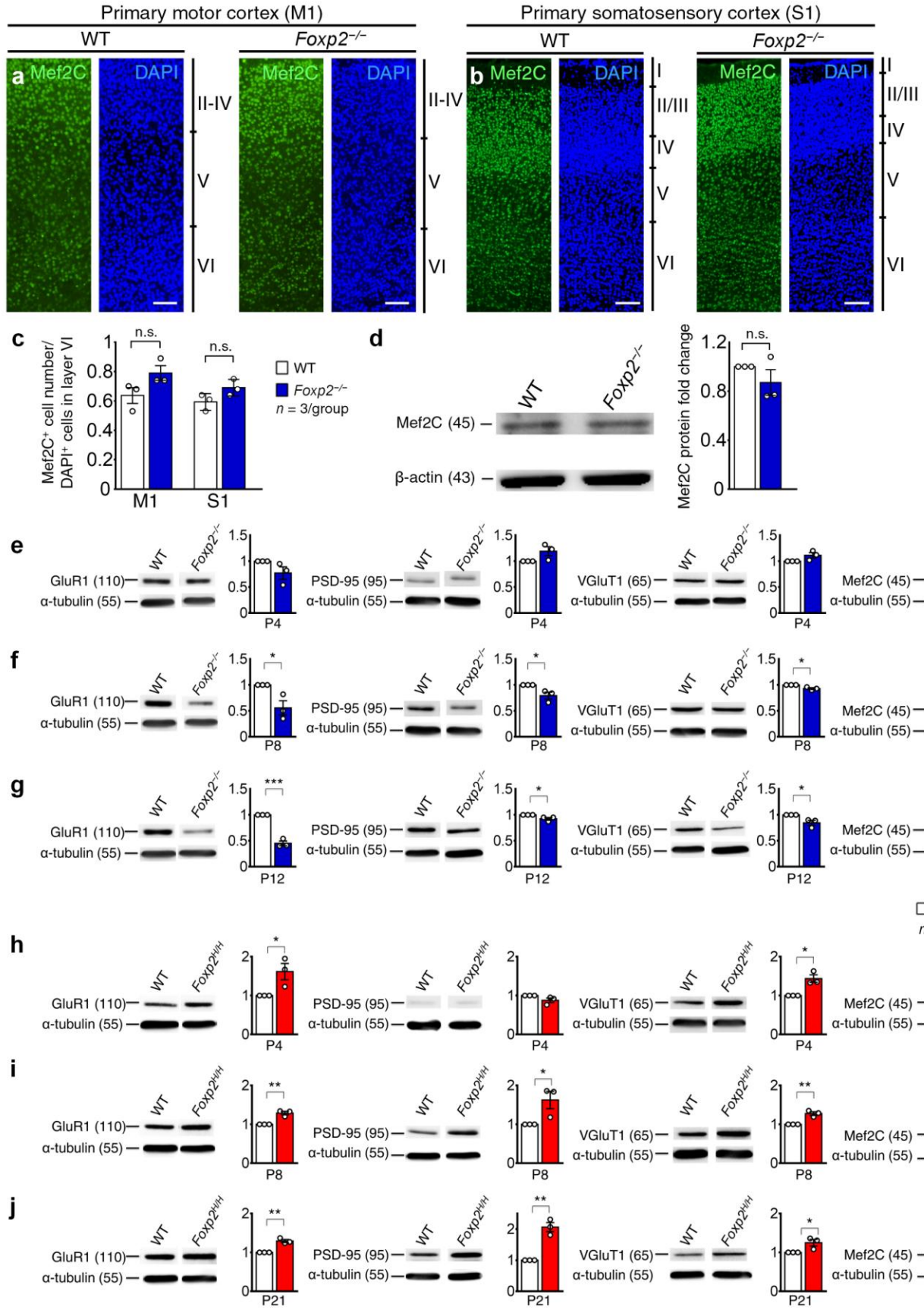

Nature Neuroscience: doi:10.1038/nn.4380

Supplementary Figure 6

Mef2C is not appreciably altered in the neocortex of *Foxp2* knockout mice, and synaptic markers and Mef2C expression are inversely correlated in the striatum of *Foxp2*$^{-/-}$ and *Foxp2*$^{H/H}$ mice during postnatal development.

(**a-c**) In Foxp2-rich layer VI of primary motor cortex (M1) and primary somatosensory cortex (S1), the density of Mef2C-positive cells is not changed significantly in *Foxp2*$^{-/-}$ knockout mice compared to *Foxp2*$^{+/+}$ wildtype control at P8 (Student's *t* test, for M1, $t_{(4)} = -2.102$, $P = 0.103$; for S1, $t_{(4)} = -2.063$, $P = 0.108$). (**d**) Western blotting shows no change in the level of Mef2C protein in the neocortex of *Foxp2*$^{-/-}$ knockout mice (Student's *t* test, $t_{(4)} = 1.243$, $P = 0.340$). (**e-g**) In *Foxp2*$^{-/-}$ mice, the levels of Mef2C and synaptic markers GluR1, PSD95 and VGluT1 are not changed at P4 (**e,** for GluR1, $t_{(4)} = 1.859$, $P = 0.204$; for PSD-95, $t_{(4)} = -2.138$, $P = 0.166$; for VGluT1, $t_{(4)} = -2.086$, $P = 0.105$; for Mef2C, $t_{(4)} = 0.167$, $P = 0.883$). By P8, GluR1, PSD95 and VGluT1 are decreased, but Mef2C is increased (**f,** for GluR1, $t_{(4)} = 3.169$, $P = 0.034$; for PSD-95, $t_{(4)} = 3.055$, $P = 0.038$; for VGluT1, $t_{(4)} = 4.114$, $P = 0.015$; for Mef2C, $t_{(4)} = -2.919$, $P = 0.043$). This pattern of protein expression is maintained at P12 (**g,** for GluR1, $t_{(4)} = 11.890$, $P = 0.000287$; for PSD-95, $t_{(4)} = 2.823$, $P = 0.048$; for VGluT1, $t_{(4)} = 3.226$, $P = 0.032$; for Mef2C, $t_{(4)} = -2.789$, $P = 0.049$). (**h-j**) In *Foxp2*$^{H/H}$ mice, synaptic markers GluR1 and VGluT1 are increased, but Mef2C is decreased at P4 (**h,** for GluR1, $t_{(4)} = -2.952$, $P = 0.042$; for PSD-95, $t_{(4)} = 2.020$, $P = 0.113$; for VGluT1, $t_{(4)} = -4.518$, $P = 0.011$; for Mef2C, $t_{(4)} = 5.838$, $P = 0.004$). By P8, Mef2C is also decreased, but VGluT1, PSD95 and GluR1 are increased (**i,** for GluR1, $t_{(4)} = -6.268$, $P = 0.003$; for PSD-95, $t_{(4)} = -2.826$, $P = 0.048$; for VGluT1, $t_{(4)} = -5.797$, $P = 0.004$; for Mef2C, $t_{(4)} = 3.392$, $P = 0.027$). This pattern of altered protein expression persisted through P21 (**j,** or GluR1, $t_{(4)} = -7.169$, $P = 0.002$; for PSD-95, $t_{(4)} = -7.396$, $P = 0.002$; for VGluT1, $t_{(4)} = -2.958$, $P = 0.042$; for Mef2C, $t_{(4)} = 10.873$, $P = 0.000406$). $^{*}P < 0.05$, $^{**}P < 0.01$; $^{***}P < 0.001$. Error bars represent s.e.m. Images and data represent three mice per genotype.

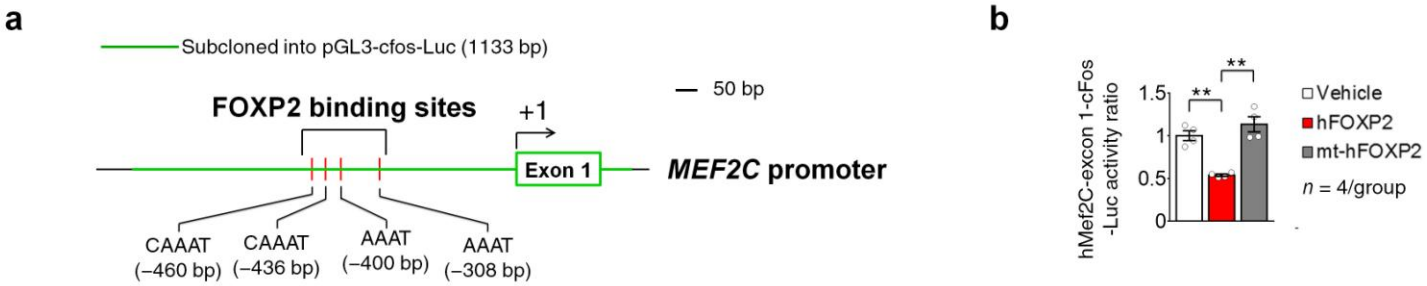

Supplementary Figure 7

FOXP2 represses human *MEF2C* reporter gene activity.
(**a**) Schematic drawing of 5' flanking region (−872 to 261 bp, transcription initiation site: +1) of human *MEF2C* gene containing putative hFOXP2 binding sites. (**b**) Co-transfection of the human *MEF2C-c-fos-Luc* reporter gene together with *hFOXP*2, but not co-transfection with *hFOXP2*^{R553H} mutant (mt-hFOXP2), suppresses Luc reporter gene activity in SH-SY5Y cells. Data represent four repeats. Student's *t* test, Mock vs. hFoxp2, $t_{(6)} = 8.032$, $P = 0.003$; hFoxp2 vs. mtFoxp2, $t_{(6)} = -6.723$, $P = 0.006$. *$P < 0.05$, **$P < 0.01$. Error bars represent s.e.m.

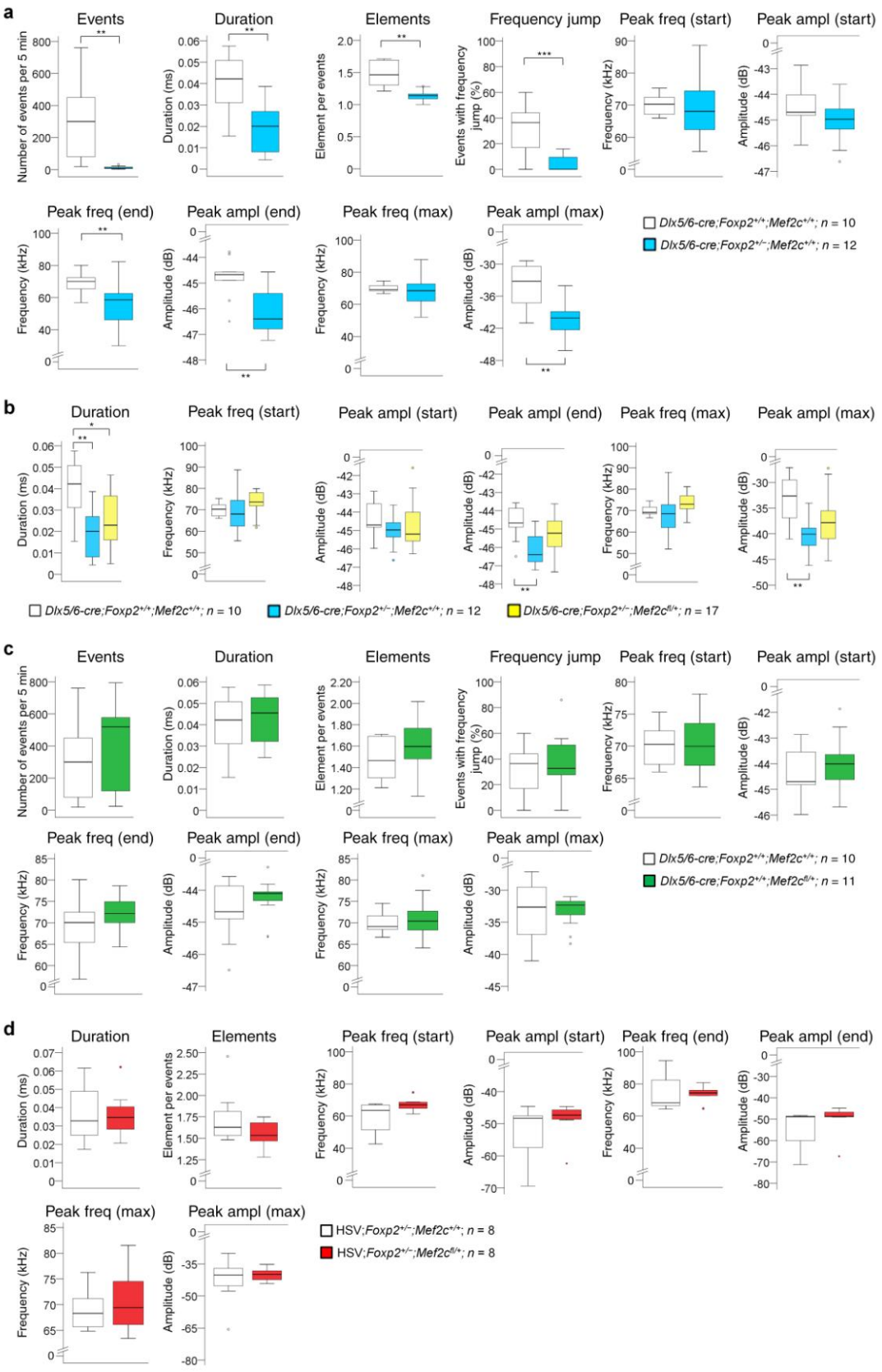

Nature Neuroscience: doi:10.1038/nn.4380

Supplementary Figure 8

Analyses of multiple USVs in different *Foxp2* mutant mice.
(**a**) Reduction of multiple USVs in *Foxp2*$^{+/-}$ heterozygous mice at P8. Compared to *Dlx5/6-cre;Foxp2*$^{+/+}$*;Mef2c*$^{+/+}$ mice (white, *Foxp2*$^{+/+}$ wildtype), the *Dlx5/6-cre;Foxp2*$^{+/-}$*;Mef2c*$^{+/+}$ mice (blue, *Foxp2*$^{+/-}$ heterozygotes) are defective in multiple USV characteristics, including the number of calls (events; Student's *t* test, $t_{(20)} = 3.902$, $P = 0.004$), duration of each call ($t_{(20)} = 3.870$, $P = 0.001$), number of elements in each call ($t_{(20)} = 4.965$, $P = 0.0001$), proportion of calls with frequency jump ($t_{(20)} = 4.494$, $P = 0.001$), peak frequency at end of calls ($t_{(20)} = 2.765$, $P = 0.012$), peak amplitude at end of calls ($t_{(20)} = 3.615$, $P = 0.002$) and maximum peak amplitude ($t_{(20)} = 3.782$, $P = 0.001$). Peak frequency at start ($t_{(20)} = 0.316$, $P = 0.756$), peak amplitude at start ($t_{(20)} = 1.364$, $P = 0.188$) and maximum peak frequency ($t_{(20)} = 0.790$, $P = 0.443$) are not affected. (**b**) Some USV characteristics are not affected by inactivation of one allele of *Mef2c*$^{fl/+}$ in *Dlx5/6-cre;Foxp2*$^{+/-}$ heterozygotes (yellow). The duration of each call (one-way ANOVA followed by Tukey's HSD *post hoc* test, $F_{(2, 36)} = 7.317$, $P = 0.002$), peak frequency at start ($F_{(2, 36)} = 1.590$, $P = 0.218$), peak amplitude at start ($F_{(2, 36)} = 0.861$, $P = 0.431$), peak amplitude at end ($F_{(2, 36)} = 5.729$, $P = 0.007$), maximum peak frequency ($F_{(2, 36)} = 2.705$, $P = 0.080$) and maximum peak amplitude ($F_{(2, 36)} = 6.949$, $P = 0.003$) of USV are not statistically altered in *Foxp2* heterozygotes mice in which *Mef2c* is heterozygous (*Dlx5/6-cre;Foxp2*$^{+/-}$*;Mef2c*$^{fl/+}$) relative to USVs in *Dlx5/6-cre;Foxp2*$^{+/-}$*;Mef2c*$^{+/+}$ mice in which *Mef2c* is wildtype. (**c**) USV analyses of P8 *Dlx5/6-cre;Foxp2*$^{+/+}$*;Mef2c*$^{fl/+}$ (green) and *Dlx5/6-cre;Foxp2*$^{+/+}$*;Mef2c*$^{+/+}$ (white) mice. No significant changes in USV features are found between these mice (Student's *t* test, for events, $t_{(19)} = -0.664$, $P = 0.515$; for duration, $t_{(19)} = -0.552$, $P = 0.587$; for elements, $t_{(19)} = -1.099$, $P = 0.286$; for frequency jump, $t_{(19)} = -0.720$, $P = 0.480$; for peak frequency at start, $t_{(19)} = -0.031$, $P = 0.976$; for peak amplitude at start, $t_{(19)} = -0.921$, $P = 0.369$; for peak frequency at end, $t_{(19)} = -0.968$, $P = 0.345$; for peak amplitude at end, $t_{(19)} = -1.263$, $P = 0.222$; for maximum peak frequency, $t_{(19)} = -0.747$, $P = 0.464$; for maximum peak amplitude, $t_{(19)} = -0.031$, $P = 0.976$). (**d**) Some USV characteristics are not affected in HSV-Cre-GFP*;Foxp2*$^{+/-}$*;Mef2c*$^{fl/+}$ mice. The duration of each call (Student's *t* test, $t_{(14)} = 0.046$, $P = 0.964$), elements ($t_{(14)} = 1.483$, $P = 0.160$), peak frequency at start ($t_{(14)} = -2.104$, $P = 0.054$), peak amplitude at start ($t_{(14)} = 0.096$, $P = 0.350$), peak frequency at end ($t_{(14)} = 0.053$, $P = 0.959$), peak amplitude at end ($t_{(14)} = -0.943$, $P = 0.362$), maximum peak frequency ($t_{(14)} = -0.663$, $P = 0.518$) and maximum peak amplitude ($t_{(14)} = -0.650$, $P = 0.526$) of USVs are not statistically altered in P8 HSV-Cre-GFP*;Foxp2*$^{+/-}$*;Mef2c*$^{fl/+}$ mice (red) compared to control HSV-Cre-GFP*;Foxp2*$^{+/-}$*;Mef2c*$^{+/+}$ mice (white). Box plots show the median (horizontal line in the box), range between the 25th and 75th percentiles (box), and 1.5 times this interquartile range (T-bars). Outlying values are marked as circles. $^{**}P < 0.01$; $^{***}P < 0.001$. Data represent at least 8 mice per genotype.

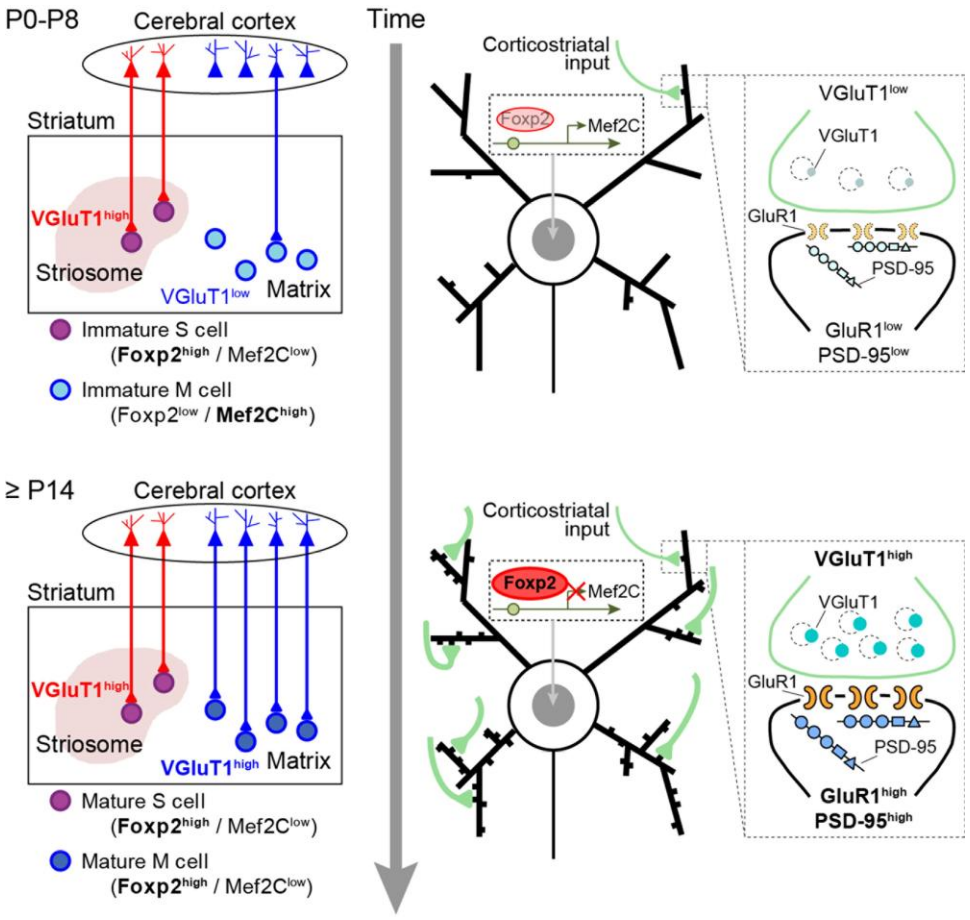

Supplementary Figure 9

Schematic drawings summarizing striatal Foxp2–Mef2C interaction in regulating synaptogenesis and vocalization. (**left**) VGluT1^{+} corticostriatal axon terminals preferentially innervate immature striosomal SPNs (Foxp2^{high}/Mef2C^{low}) but not immature matrix SPNs (Foxp2^{low}/Mef2C^{high}) at P0-P8 (**top**). By P14, corticostriatal axons innervate both striosomal and matrix cells (Foxp2^{high}/Mef2C^{low}, **bottom**). (**right**) Diagram depicting hypothesis that Foxp2 functions as a molecular key to unlock Mef2C-mediated inhibition of synapse formation in SPNs during development. When Foxp2 levels are low, Mef2C is de-repressed to inhibit corticostriatal synaptogenesis (**top**). When Foxp2 levels are high, Foxp2 represses Mef2C to promote corticostriatal synaptogenesis, which is linked to facilitation of USV production (**bottom**).

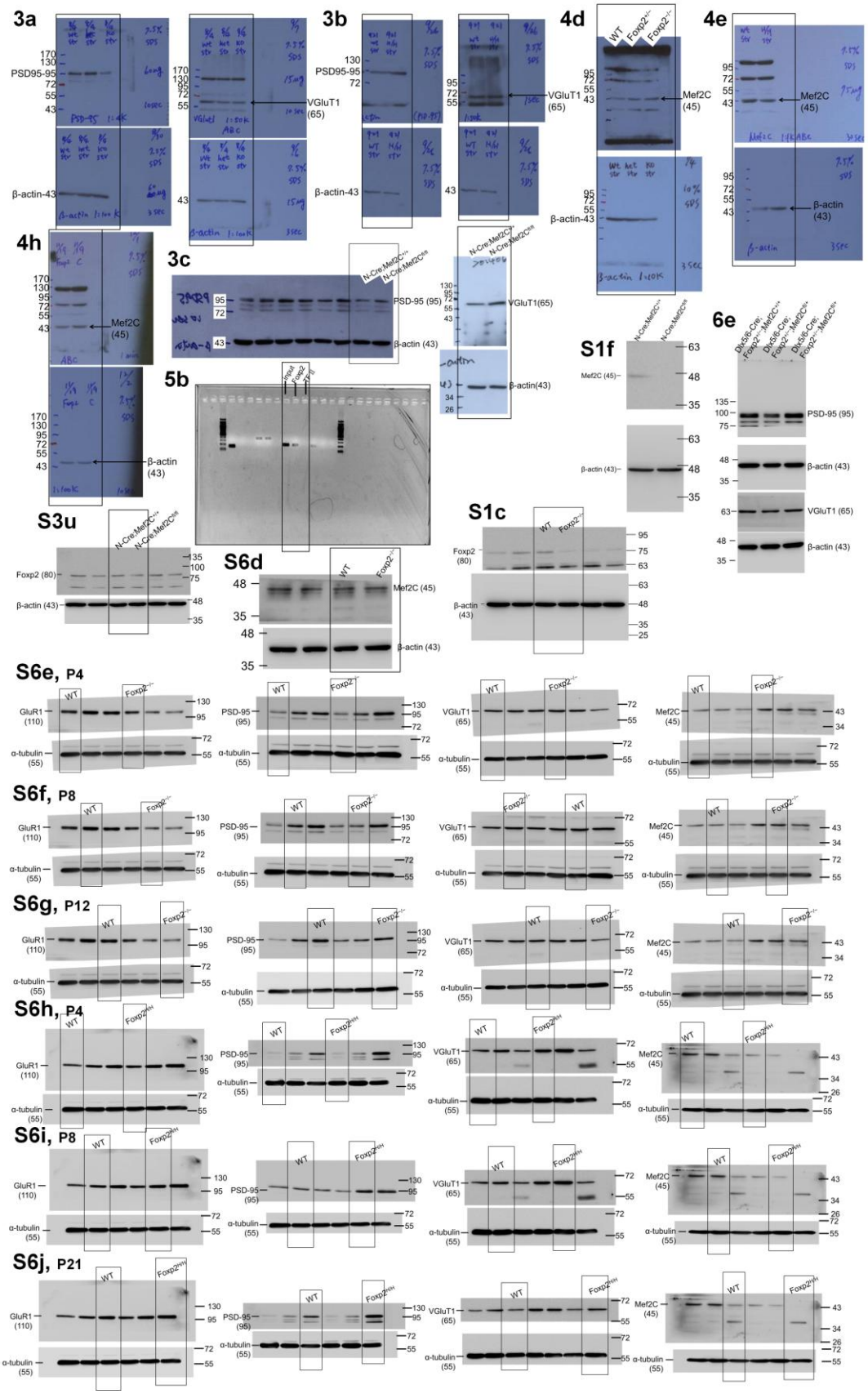

Nature Neuroscience: doi:10.1038/nn.4380

Supplementary Figure 10

Full-length gels and blots.
The original Western blots of the cropped blots shown in **Figures 3a-c, 4d,e,h and 6e**, and in **Supplementary Figures 1c,f, 3u and 6d-j**, and the original gel shown in **Figure 5b**.

Supplementary Table 1 Dendritic spines are decreased in SPNs of *Foxp2*$^{-/-}$ mice

Region	Genotype	Stubby	Thin/filopodia	Mushroom	Branched	Multiple branched	Atypical	Sum
Dorsolateral striatum	Wildtype	3.40 ± 0.13	3.28 ± 0.12	1.72 ± 0.10	0.57 ± 0.07	0.00 ± 0.00	0.13 ± 0.05	9.10 ± 0.15
	Foxp2$^{+/-}$	3.68 ± 0.10	3.38 ± 0.13	1.42 ± 0.08*	0.35 ± 0.0*	0.00 ± 0.00	0.18 ± 0.04	9.02 ± 0.14
	Foxp2$^{-/-}$	3.37 ± 0.07	2.80 ± 0.10**	1.12 ± 0.07***	0.33 ± 0.06*	0.00 ± 0.00	0.15 ± 0.05	7.83 ± 0.14***
Dorsomedial striatum	Wildtype	3.38 ± 0.12	3.48 ± 0.12	1.23 ± 0.08	0.56 ± 0.07	0.00 ± 0.00	0.13 ± 0.05	8.80 ± 0.14
	Foxp2$^{+/-}$	3.55 ± 0.10	3.32 ± 0.10	1.10 ± 0.08	0.30 ± 0.07*	0.00 ± 0.0	0.22 ± 0.05	8.48 ± 0.12
	Foxp2$^{-/-}$	3.30 ± 0.11	2.71 ± 0.08***	0.73 ± 0.07***	0.27 ± 0.05**	0.00 ± 0.00	0.10 ± 0.04	7.12 ± 0.13***

Means ± s.e.m. per 10 µm; **P* < 0.05, ***P* < 0.01, ****P* < 0.001, compared to wildtype; *n* = 30 cells from 3 mice in each group.

Nature Neuroscience: doi:10.1038/nn.4380

Supplementary Table 2 Dendritic spines are increased in SPNs of *Foxp2*$^{H/H}$ mice

Region	Genotype	Stubby	Thin/filopodia	Mushroom	Branched	Multiple branched	Atypical	Sum
Dorsolateral striatum	Wildtype	3.65 ± 0.10	3.45 ± 0.10	1.13 ± 0.07	0.46 ± 0.07	0.02 ± 0.01	0.20 ± 0.05	8.91 ± 0.16
	Foxp2$^{H/H}$	3.57 ± 0.10	3.80 ± 0.12*	1.37 ± 0.08*	0.77 ± 0.11*	0.22 ± 0.05**	0.15 ± 0.04	9.86 ± 0.16***
Dorsomedial striatum	Wildtype	3.50 ± 0.10	3.18 ± 0.08	1.05 ± 0.07	0.42 ± 0.07	0.00 ± 0.00	0.20 ± 0.05	8.35 ± 0.13
	Foxp2$^{H/H}$	3.57 ± 0.11	3.47 ± 0.01*	1.22 ± 0.10	0.05 ± 0.07	0.05 ± 0.03	0.18 ± 0.05	9.01 ± 0.15**

Means ± s.e.m. per 10 µm; *P < 0.05, **P < 0.01, ***P < 0.001, compared to wildtype; n = 30 cells from 3 mice in each group.

Nature Neuroscience: doi:10.1038/nn.4380

Supplementary Table 3 Dendritic spines are increased in SPNs of *Nestin-Cre;Mef2C$^{fl/+}$ and Nestin-Cre;Mef2C$^{fl/fl}$* mice

Region	Genotype	Stubby	Thin/filopodia	Mushroom	Branched	Multiple branched	Atypical	Sum
Dorsolateral striatum	*Nestin-Cre; Mef2C$^{+/+}$*	2.07 ± 0.13	3.05 ± 0.13	0.79 ± 0.07	0.72 ± 0.06	0.02 ± 0.01	0.37 ± 0.06	7.02 ± 0.20
	Nestin-Cre;Mef2C$^{fl/+}$	2.23 ± 0.20	3.54 ± 0.20	0.77 ± 0.09	1.21 ± 0.11***	0.21 ± 0.06**	0.94 ± 0.12***	8.91 ± 0.26***
	Nestin-Cre; Mef2C$^{fl/fl}$	4.11 ± 0.22***	3.30 ± 0.19	1.12 ± 0.09*	1.00 ± 0.07*	0.09 ± 0.03	0.57 ± 0.07	10.19 ± 0.31***
Dorsomedial striatum	*Nestin-Cre; Mef2C$^{+/+}$*	1.86 ± 0.10	2.58 ± 0.16	0.54 ± 0.05	0.72 ± 0.07	0	0.50 ± 0.07	6.14 ± 0.20
	Nestin-Cre;Mef2C$^{fl/+}$	1.87 ± 0.15	4.09 ± 0.28***	0.54 ± 0.10	1.47 ± 0.14	0.17 ± 0.05***	1.05 ± 0.13***	9.18 ± 0.26***
	Nestin-Cre; Mef2C$^{fl/fl}$	4.27 ± 0.26***	3.54 ± 0.24	1.11 ± 0.10***	1.14 ± 0.09	0.07 ± 0.21	0.67 ± 0.07	10.93 ± 0.36***

Means ± s.e.m. per 10 µm; *P < 0.05, **P < 0.01, ***P < 0.001, compared to *Nestin-Cre; Mef2C$^{+/+}$*; Dorsolateral striatum: n = 38 cells from 3 mice in *Nestin-Cre;Mef2C$^{+/+}$* group, n = 38 cells from 3 mice in *Nestin-Cre;Mef2C$^{fl/+}$* group, n = 33 cells from 3 mice in *Nestin-Cre;Mef2C$^{fl/fl}$* group; Dorsomedial striatum: n = 47 cells from 3 mice in *Nestin-Cre;Mef2C$^{+/+}$* group, n = 30 cells from 3 mice in *Nestin-Cre;Mef2C$^{fl/+}$* group, n = 36 cells from 3 mice in *Nestin-Cre;Mef2C$^{fl/fl}$* group.

Nature Neuroscience: doi:10.1038/nn.4380

Supplementary Table 4 Increased dendritic spines in SPNs of *Dlx5/6Cre;Foxp2*$^{+/-}$*;Mef2C*$^{fl/+}$ mice

Region	Genotype	Stubby	Thin/filopodia	Mushroom	Branched	Multiple branched	Atypical	Sum
Dorsolateral striatum	*Dlx5/6Cre; Foxp2*$^{+/+}$*; Mef2C*$^{+/+}$	4.25 ± 0.32	5.33 ± 0.32	1.09 ± 0.13	0.97 ± 0.13	0.19 ± 0.06	0.54 ± 0.09	12.38 ± 0.44
	Dlx5/6Cre; Foxp2$^{+/-}$*; Mef2C*$^{+/+}$	3.25 ± 0.18*	2.90 ± 0.29***	0.74 ± 0.11	0.34 ± 0.06***	0.07 ± 0.03	0.37 ± 0.08	7.77 ± 0.35***
	Dlx5/6Cre; Foxp2$^{+/-}$*; Mef2C*$^{fl/+}$	4.29 ± 0.32	3.94 ± 0.34*	1.19 ± 0.12	0.73 ± 0.09	0.09 ± 0.04	0.80 ± 0.11	10.86 ± 0.47*
Dorsomedial striatum	*Dlx5/6Cre; Foxp2*$^{+/+}$*; Mef2C*$^{+/+}$	4.30 ± 0.34	5.33 ± 0.50	0.73 ± 0.12	0.77 ± 0.15	0.11 ± 0.04	0.96 ± 0.13	12.20 ± 0.53
	Dlx5/6Cre; Foxp2$^{+/-}$*; Mef2C*$^{+/+}$	3.35 ± 0.27*	1.98 ± 0.18***	0.22 ± 0.04***	0.15 ± 0.01***	0.01 ± 0.08	0.54 ± 0.08*	6.42 ± 0.26***
	Dlx5/6Cre; Foxp2$^{+/-}$*; Mef2C*$^{fl/+}$	4.51 ± 0.31	3.20 ± 0.37**	0.3 ± 0.07	0.35 ± 0.07*	0.06 ± 0.03	0.66 ± 0.11	9.27 ± 0.33***

Means ± s.e.m. per 10 μm; **P* < 0.05, ***P* < 0.01, ****P* < 0.001, compared to *Dlx5/6Cre;Foxp2*$^{+/+}$*;Mef2C*$^{+/+}$; Dorsolateral striatum, *n* = 30 cells from 3 mice in *Dlx5/6Cre;Foxp2*$^{+/+}$*;Mef2C*$^{+/+}$group, *n* = 36 cells from 3 mice in *Dlx5/6Cre; Foxp2*$^{+/-}$*;Mef2C*$^{+/+}$group, *n* = 35 cells from 3 mice in *Dlx5/6Cre; Foxp2*$^{+/-}$*;Mef2C*$^{fl/+}$ group; Dorsomedial striatum, *n* = 30 cells from 3 mice in each group.

Nature Neuroscience: doi:10.1038/nn.4380